Building Fuzzy Elevation Maps from a Ground-based 3D Laser Scan for Outdoor Mobile Robots

Anthony Mandow, Tomás J. Cantador, Antonio J. Reina,
Jorge L. Martínez, Jesús Morales, and Alfonso García-Cerezo

Universidad de Málaga – Andalucía Tech
Departamento de Ingeniería de Sistemas y Automática, 29071 Málaga, Spain.
Email: amandow[@]uma.es

Abstract - The paper addresses terrain modeling for mobile robots with fuzzy elevation maps by improving computational speed and performance over previous work on fuzzy terrain identification from a three-dimensional (3D) scan. To this end, spherical sub-sampling of the raw scan is proposed to select training data that does not filter out salient obstacles. Besides, rule structure is systematically defined by considering triangular sets with an unevenly distributed standard fuzzy partition and zero order Sugeno-type consequents. This structure, which favors a faster training time and reduces the number of rule parameters, also serves to compute a fuzzy reliability mask for the continuous fuzzy surface. The paper offers a case study using a Hokuyo-based 3D rangefinder to model terrain with and without outstanding obstacles. Performance regarding error and model size is compared favorably with respect to a solution that uses quadric-based surface simplification (QSlim).

Keywords: Elevation maps, mobile robots, 3D scanners, fuzzy modeling

---

Citation Information:

Mandow, A; Cantador, T.J.; Reina, A.J.; Martínez, J.L.; Morales, J.; García-Cerezo, A.
"Building Fuzzy Elevation Maps from a Ground-based 3D Laser Scan for Outdoor Mobile Robots,"
(2016) Advances in Intelligent Systems and Computing, vol. 418.

```
@ARTICLE{Mandow:2016,
author={Mandow, A and Cantador, T.J. and Reina, A.J. and Martínez, J.L. and Morales, J. and García-Cerezo, A.},
title={Building Fuzzy Elevation Maps from a Ground-based {3D} Laser Scan for Outdoor Mobile Robots},
journal={Advances in Intelligent Systems and Computing},
year={2016},
volume={418},
}
```

Building Fuzzy Elevation Maps from a Ground-based 3D Laser Scan for Outdoor Mobile Robots

Anthony Mandow, Tomás J. Cantador, Antonio J. Reina,
Jorge L. Martínez, Jesús Morales, and Alfonso García-Cerezo

Universidad de Málaga, Andalucía Tech
Dpto. Ingeniería de Sistemas y Automática, 29071 Málaga, Spain
amandow@uma.es;http://www.uma.es/isa

Abstract. The paper addresses terrain modeling for mobile robots with fuzzy elevation maps by improving computational speed and performance over previous work on fuzzy terrain identification from a three-dimensional (3D) scan. To this end, spherical sub-sampling of the raw scan is proposed to select training data that does not filter out salient obstacles. Besides, rule structure is systematically defined by considering triangular sets with an unevenly distributed standard fuzzy partition and zero order Sugeno-type consequents. This structure, which favors a faster training time and reduces the number of rule parameters, also serves to compute a fuzzy reliability mask for the continuous fuzzy surface. The paper offers a case study using a Hokuyo-based 3D rangefinder to model terrain with and without outstanding obstacles. Performance regarding error and model size are compared favorably with respect to a solution that uses quadric-based surface simplification (QSlim).

Keywords: Elevation maps, mobile robots, 3D scanners, fuzzy modeling

1 Introduction

Environment mapping is a key issue in mobile robots targeted to unstructured terrains [1, 2]. In this sense, three-dimensional (3D) laser scans provide valuable information for applications such as planetary exploration [3–5] or urban search and rescue [6, 7]. However, as point clouds require coping with a huge amount of spatial data, a simplified and compact representation of navigable terrain is necessary for both motion planning [8] and tele-operation [9].

Elevation maps offer a compact 2.5-dimensional model of terrain surface. In robotics, elevation has been generally represented by regular grids [10–12] or by irregular triangular meshes [4, 13]. Removal of artifacts and mesh simplification algorithms, like mesh decimation [14] and quadric-based polygonal surface simplification (QSlim) vertex clustering [15], can improve the compactness and reliability of these maps [8]. Nevertheless, as tesselated models have limitations in the face of incomplete and uncertain sensor data, some works have proposed

using tools that can model elevation in a more robust and natural way. In geographic information systems (GIS), fuzzy logic has been applied to elevation maps for incorporating height uncertainty [16] and assessing visibility between pairs of points [17]. In mobile robotics, elevation grids have been processed with fuzzy rules to assess traversability [18, 19]. Gaussian processes have also been proposed to model terrain from uncertain and incomplete sensor data [20]. Adaptive Network-based Fuzzy Inference Systems (ANFIS) [21] has been employed to recognize objects like trees and buildings from aerial stereo images [22]. Moreover, ANFIS was preliminarily proposed to obtain fuzzy elevation maps of natural terrain from ground-based 3D data [23]. These elevation maps have been already employed for assessing traversability and local path planning [24].

The main contribution of this paper is extending [23] to improve computational speed and performance. To this end, two major modifications have been introduced: *i*) spherical sub-sampling [25] is used to select proper training data from a raw point cloud, and *ii*) rule parameters have been systematically defined by considering triangular sets with standard fuzzy partition [26] as well as zero order Sugeno-type inference. Furthermore, the capability to model a salient obstacle on the terrain surface has been considered in a case study using a 3D Hokuyo-based range-finder. Besides, performance regarding error and computation time are compared with a solution based on the QSlim algorithm.

Following this introduction, section II presents the fuzzy terrain modeling method. Then, section III describes the experiments including comparisons with QSlim. Finally, Section IV offers conclusions and future work.

2 Fuzzy terrain modeling method

The proposed fuzzy terrain modeling method is outlined in Fig. 1. The input is a range image from a single 3D scan. It is assumed that the local frame of the 3D rangefinder has its Y and Z axes pointing forwards and upwards, respectively (see Fig. 2). The goal of the method is producing a local elevation map in which ground surface can be represented as a function $z = H(x, y)$, where x and y are the Cartesian coordinates on the XY plane and z is the corresponding elevation. The following subsections develop the major parts of this algorithm.

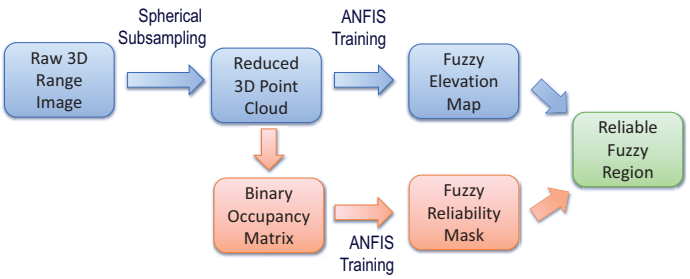

Fig. 1. Fuzzy point cloud terrain modeling algorithm.

2.1 Point sub-sampling

The purpose of point sub-sampling is to produce a reduced set of representative training points in Cartesian coordinates (x, y, z). The reason for sub-sampling is twofold: improving the speed of fuzzy identification and homogenizing the spatial distribution of training data. In [23], sub-sampling was performed by selecting the highest point within grid cells of a sufficiently high resolution. This approach provides a representative set of points for a smooth terrain but is not so effective to model salient obstacles, such as tree trunks or rocks, which can be filtered by the fuzzy identification method when represented by a small number of samples. Furthermore, finding the maximum value within each cell entails the computational load of processing all scan points in Cartesian coordinates.

Alternatively, spherical sub-sampling [25] performs a fast range-independent data reduction for 3D rangefinders that combine a 2D scan with an additional rotation, as usually found in mobile robots [27]. Moreover, by equalizing the measure-direction density, spherical sub-sampling maintains a proportion of measurements accumulated by salient obstacles, so their contribution can be relevant when adjusting a fuzzy surface. Thus, Cartesian coordinates are only computed for sub-sampled points.

The field of view of the 3D sensor is defined by the scope of both scan angles: Φ for the 2D scan and Ψ for the additional rotation, as shown in Fig. 2(left). Then, angular resolution is given by $\Delta\phi$ and $\Delta\psi$ for the first and second rotations, respectively. The amount of data reduction of spherical sub-sampling is established by an equalization factor $0 < p \leq 1$. The equalized angular resolution of the sub-sampled scan (see Fig. 2(right)) is given by $\Delta\theta_s$ as:

$$\Delta\theta_s = \frac{\max(\Delta\psi, \Delta\phi)}{p}. \tag{1}$$

In this way, by setting $p = 1$, the measure-direction density is equalized with the coarsest resolution (either $\Delta\phi$ or $\Delta\psi$) actually provided by the sensor.

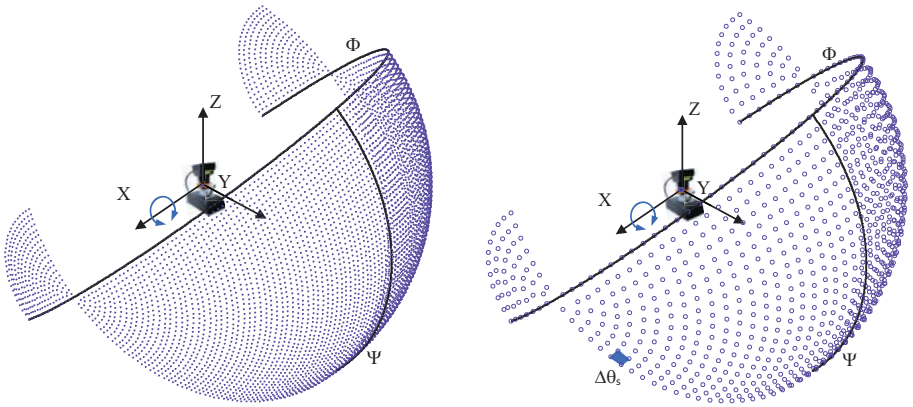

Fig. 2. Measure-direction density. Left: raw scan; right: spherical point sub-sampling.

2.2 Neuro-Fuzzy Training

The set of sub-sampled Cartesian points is used to adjust a fuzzy model $z = H(x, y)$. Particularly, neuro-fuzzy ANFIS modeling [21] is adopted to identify a fuzzy model with Sugeno inference. ANFIS yields the rule consequents for a given fuzzy structure where membership functions (MFs) have to be specified for each input variable.

The definition of MFs has an impact on the model size; i.e., on the number of parameters. One interesting property of the standard fuzzy partition (SPF) is that triangular or trapezoidal MFs share parameter values with neighbor MFs [26]. In an SPF, the i^{th} MF $\mathbf{F}_i$ defined for a given variable u in the universe U is convex, normal, and it only overlaps with its neighboring fuzzy sets, in such a way that:

$$\forall u \in U, \quad \sum_{\forall i} \mathbf{F}_i(u) = 1. \tag{2}$$

When defining the fuzzy structure, a greater number of MFs improves terrain adjustment at the cost of processing a greater number of rules. This conflict can be coped with by considering that higher detail is more important for the regions that are closest to the robot. Thus, an uneven membership function distribution can provide an appropriate fuzzy structure if the density of MFs for variables x and y is specified depending on the distance to the sensor [23].

Let us define the universe $U_x = [-u_{max}, u_{max}]$ for variable x, and $U_y = [0, u_{max}]$ for y, which corresponds to a $2u_{max} \times u_{max}$ rectangular area in the forward direction of the sensor. Then, uneven SPF MFs can be defined by computing the peak parameter f_i of each triangular MF $\mathbf{F}_i$ (i.e., $F_i(f_i) = 1$) as:

$$f_i = \text{sign}(i) \left(\frac{r^{|i|} - 1}{r^k - 1} \right) u_{max} \tag{3}$$

where $r > 1$ is the expansion ratio and $i = -k, ..., 0, 1, ..., k$ for the x variable and $i = 0, 1, ..., k$ for y. This definition yields $(2k + 1)$ MFs for x and $(k + 1)$ MFs for y. This means $(2k + 1) \times (k + 1)$ rules.

Furthermore, the order of Sugeno inference affects training time as well as the number of rule parameters. In [23], first-order consequents G_i were considered for every rule i as:

$$G_i(x, y) = a_i + b_i\, x + c_i\, y, \tag{4}$$

where three parameters (a_i, b_i, c_i) per rule had to be identified. Alternatively, using zero-order Sugeno consequents:

$$G_i(x, y) = a_i \tag{5}$$

requires just one parameter per rule, as $b_i = c_i = 0$. First order Sugeno can be useful for ome applications, like interpolating between piecewise linear controllers, but zero-order consequents can provide good accuracy when approximating nonlinear functions [28]. Furthermore, the output of a zero-order Sugeno model is smooth as long as neighboring MFs in the antecedents are overlapped, as in SPF [29]. Therefore, zero-order Sugeno consequents are proposed as an effective solution for this application.

2.3 Fuzzy Reliability Mask

ANFIS renders a fuzzy surface that can be evaluated for any (x, y) pair in the universe of discourse. This surface filters sensor noise and interpolates missing data from small shadowed areas but can provide erroneous estimations in larger regions with no input data. Since shadowed regions are frequent in ground-based scans of natural terrain proper use of the elevation map requires reliability assessment, which is a fuzzy concept in itself.

A fuzzy reliability mask is proposed as a continuous function $v = V(x, y)$, where $v \in [0, 1]$ for inputs $x \in U_x$ and $y \in U_y$. This function can be trained with ANFIS with the same fuzzy structure as in the elevation map. For this purpose, an occupancy binary matrix is computed from the sub-sampled points. This matrix represents an XY grid with a uniform resolution δ, where ones and zeroes are assigned to cells with or without points, respectively. Then, the training data consists of the set of all matrix values with the corresponding cell center XY coordinates. In the resulting fuzzy model, values of $v = V(x, y)$ close to one indicate high reliability of $H(x, y)$, whereas values close to zero mean unreliable regions.

3 Experimental results

3.1 Experimental Setup

This section discusses the application of fuzzy elevation modeling using 3D range images from a natural terrain —see Fig. 3(left). Four different scans obtained from the same sensor pose are considered: without obstacles, and with a person standing at three different positions with respect to the sensor frame: *close-front*, at a distance of 2.94 m with approximate XY coordinates $(0.05\text{m}, 2.94\text{m})$; *close-side*, at 3.94 m with $(3.49\text{m}, 1.83\text{m})$; and *far*, at 7.26 m with $(-0.14\text{m}, 7.26\text{m})$. Computations have been performed by a QuadCore Intel Core i7 at 2.2 GHz under the Matlab environment, whose Fuzzy Toolbox includes ANFIS.

Range images have been obtained with a 3D laser scanner built by pitching a Hokuyo UTM-30LX 2D rangefinder [30] —see Fig. 3(right). This device has the following specifications: $270° \times 135°$ field of view; measurable ranges between

Fig. 3. Experimental setup. Left: outdoor scene; right: 3D laser rangefinder.

0.1 m and 30 m; horizontal resolution $\Delta\phi = 0.25°$; and vertical resolution $\Delta\psi$ is adjustable from 0.067° to 4.24°. The scan times at minimum and maximum resolution are 1.54 s and 95.75 s, respectively. In particular, 3D scans have been obtained with $\Delta\psi = 0.278°$, which is similar to $\Delta\phi$, with the sensor standing 1.0 m above the ground. This configuration produces range images with a maximum of 505036 points in 12.43 s.

3.2 Fuzzy Performance Evaluation

Performance of the proposed method has been studied for different rule numbers and sub-sampling rates. Two different fuzzy rule structures are considered by using (3) with $r = 1.3$ and a universe of discourse $u_{max} = 10$ m: First, $k = 7$ yields 15×8 rules, and second, $k = 3$ results in 7×4 rules. As for training data, several p values are compared for spherical sub-sampling. Besides, Cartesian points whose coordinates fall out of the 20 m $\times$ 10 m rectangular area have been discarded. Fig. 4 illustrates training data for the close-front obstacle case with no sub-sampling and with $p = 0.5$.

The root mean squared error (RMSE) given in Table 1 has been computed from the difference between the Z value of all raw scan points within the universe of discourse and the corresponding fuzzy model elevation. As expected, the RMSE for the 15×8 rulebase is better than the 7×4 model. Besides, fuzzy surfaces improve RMSE for smooth terrain, i.e., with no close salient obstacles. On

Table 1. Effect of spherical sub-sampling on ANFIS performance.

Obstacle	p	Training points	No. of rules	RMSE (m^2)	Time (s)	Obstacle	p	Training points	No. of rules	RMSE (m^2)	Time (s)
None	-	186767	15×8	0.0237	176.00	Far	-	185673	15×8	0.0369	174.00
			7×4	0.0413	116.00				7×4	0.0558	117.00
	1	115423	15×8	0.0237	83.63		1	114768	15×8	0.0369	80.84
			7×4	0.0420	50.63				7×4	0.0563	47.84
	0.75	65019	15×8	0.0238	43.33		0.75	64666	15×8	0.0369	41.32
			7×4	0.0421	21.33				7×4	0.0564	20.32
	0.5	28916	15×8	0.0238	22.07		0.5	28770	15×8	0.0370	21.12
			7×4	0.0421	9.07				7×4	0.0564	9.12
	0.1	1180	15×8	0.2568	11.90		0.1	1168	15×8	0.4484	10.96
			7×4	0.0451	5.90				7×4	0.0642	5.96
Close -side	-	187600	15×8	0.0951	177.00	Close -front	-	189688	15×8	0.0871	174.00
			7×4	0.1283	115.00				7×4	0.1259	119.00
	1	115525	15×8	0.0955	80.87		1	117941	15×8	0.0879	87.65
			7×4	0.1295	48.87				7×4	0.1262	50.65
	0.75	65122	15×8	0.0955	40.33		0.75	66465	15×8	0.0872	44.26
			7×4	0.1295	20.33				7×4	0.1262	21.26
	0.5	28939	15×8	0.0956	21.07		0.5	29554	15×8	0.0872	23.05
			7×4	0.1295	9.07				7×4	0.1262	10.05
	0.1	1174	15×8	0.1580	10.89		0.1	1206	15×8	0.1568	11.19
			7×4	0.1305	4.89				7×4	0.1495	5.19

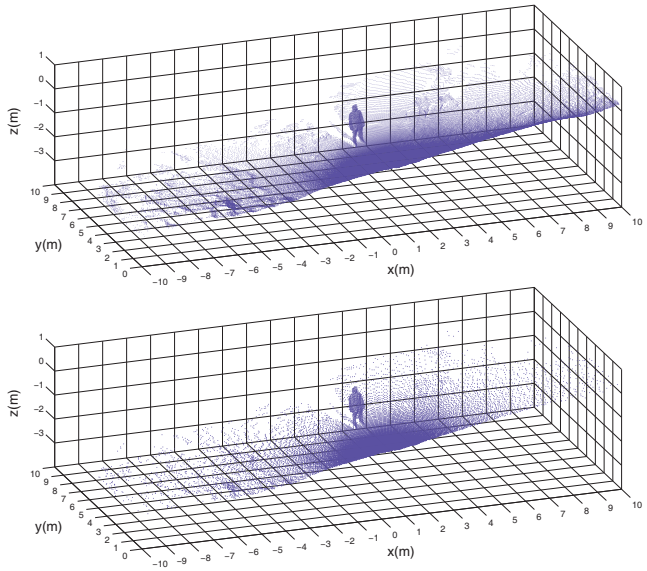

Fig. 4. Training points of the close-front obstacle scene. Top: raw scan points; Bottom: spherical sub-sampling with $p = 0.5$.

the other hand, the sub-sampling rate has an important effect on computation time, but it does not generally produce important RMSE differences within the same rule structure and scene. This indicates that spherical sub-sampling gives a representative subset of the complete scan. The only exception to these results is with 15×8 rules and sub-sampling factor 0.1, where the 120-rule fuzzy model is overadjusted to a small data sample (around 1200 points, which is only about 0.6% of the raw data set).

From this analysis, if fast rough terrain model is needed, the 7×4 rule model with 0.1 sub-sampling could offer an appropriate solution. For a compromise between acceptable model accuracy and computation time, good results are given by the 15×8 rule model with 0.5 sub-sampling (see Fig. 5).

3.3 Comparison with QSlim

The proposed method has been compared with a QSlim-based solution. QSlim [15] performs mesh surface simplification by iterative contraction of vertex pairs using plane-based error quadrics. QSlim has been employed for terrain simplification of topographical maps [31, 32]. However, QSlim cannot be directly applied to the Delaunay mesh corresponding to raw ground-based scans because of artifacts due to shadows and salient objects [8]. Therefore, preprocessing is necessary to produce a proper surface to start with. In this paper, a proper Delaunay mesh is built from the XY coordinates of the maximum height points within grid cells of resolution $\delta = 0.1\,\mathrm{m}$. The resulting mesh has been fed to the QSlim algorithm to produce models with both 100 and 1000 faces, as illustrated by Fig. 6.

Table 2 compares results obtained with the proposed method, the solution proposed in [23], and the QSlim approach. QSlim is an efficient method, so most of the computation time corresponds to preprocessing. As this preprocessing is

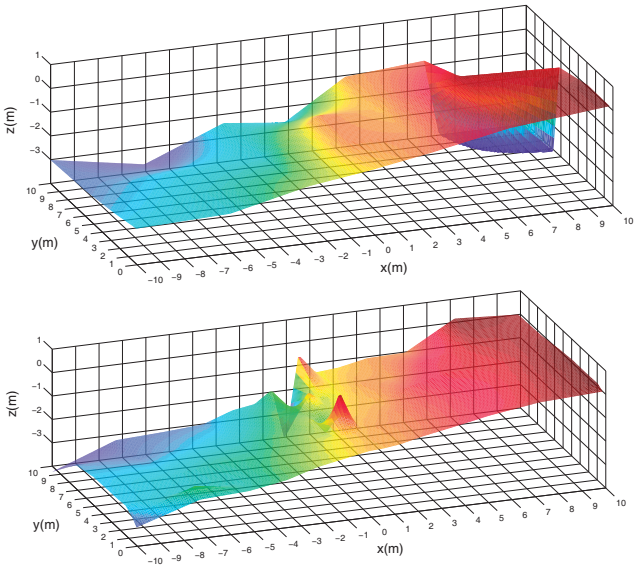

Fig. 5. Fuzzy elevation maps of the close-front obstacle scene. Top: $p = 0.1$ and 7×4 rules; bottom: $p = 0.5$ and 15×8 rules.

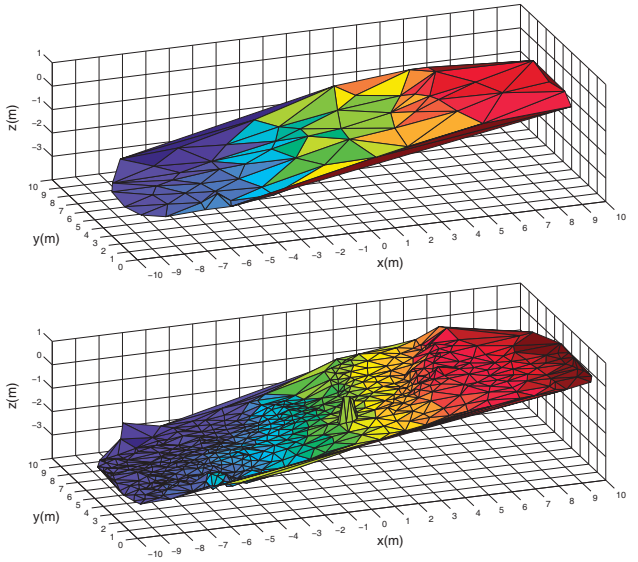

Fig. 6. QSlim maps of the close-front obstacle. Top: 100 faces; bottom: 1000 faces.

Table 2. Comparison between ANFIS and QSlim-Based Approaches.

Scene	Modeling method	Characteristics	RMSE (m^2)	Time (s)	Number of parameters
No obstacle	ANFIS	$15 \times 8, p = 0.5$	0.0238	22.07	143
		$7 \times 4, p = 0.1$	0.0451	5.90	39
		15×8 ([23])	0.0468	31.01	406
	QSlim	1000 faces	0.0250	29.17	4590
		100 faces	0.0357	29.17	483
Far obstacle	ANFIS	$15 \times 8, p = 0.5$	0.0370	21.12	143
		$7 \times 4, p = 0.1$	0.0642	5.96	39
		15×8 [23]	0.0660	31.20	406
	QSlim	1000 faces	0.0383	32.21	4572
		100 faces	0.0783	32.03	471
Close-side obstacle	ANFIS	$15 \times 8, p = 0.5$	0.0956	21.07	143
		$7 \times 4, p = 0.1$	0.1305	4.89	39
		15×8 [23]	0.1256	32.14	406
	QSlim	1000 faces	0.1349	29.14	4578
		100 faces	0.1959	29.14	477
Close-front obstacle	ANFIS	$15 \times 8, p = 0.5$	0.0872	23.05	143
		$7 \times 4, p = 0.1$	0.1495	5.19	39
		15×8 [23]	0.1303	33.07	406
	QSlim	1000 faces	0.1212	33.18	4569
		100 faces	0.2038	33.16	477

very similar to sub-sampling in [23], both methods achieve similar computation times. Spherical sub-sampling improves these times, which is particularly noticeable for 7×4 rules and $p = 0.1$. Regarding accuracy, the best results are obtained by the new method with 15×8 rules and $p = 0.5$, where RMSE is greatly improved with respect to [23] for the same number of rules. The accuracy of QSlim with 1000 faces is comparable to the best ANFIS performance with no close obstacles. However, the proposed method prevails when the model includes close obstacles. Table 2 also offers model size as the number of parameters. The proposed model requires one consequent parameter per rule. Triangular MFs are defined by three parameters, but as neighbor MFs share parameters in an SPF, only one parameter per MF is actually needed. These are improvements over [23], which required three consequent parameters and plus two values per Gaussian MF. As for QSlim, it consists of a list of vertices and a list of faces. Vertices are defined by three Cartesian coordinates and faces are specified as three vertex indices. The number of parameters of the proposed model improves [23] and clearly outperforms QSlim.

3.4 Application of the Reliability Mask

ANFIS training of fuzzy elevation from data-less regions may not be reliable and can even create artifacts, like those around $(10\,\mathrm{m}, 10\,\mathrm{m})$ in Fig. 5(top) or behind the person like in Fig. 5(bottom). Fig. 7 shows the fuzzy reliability mask

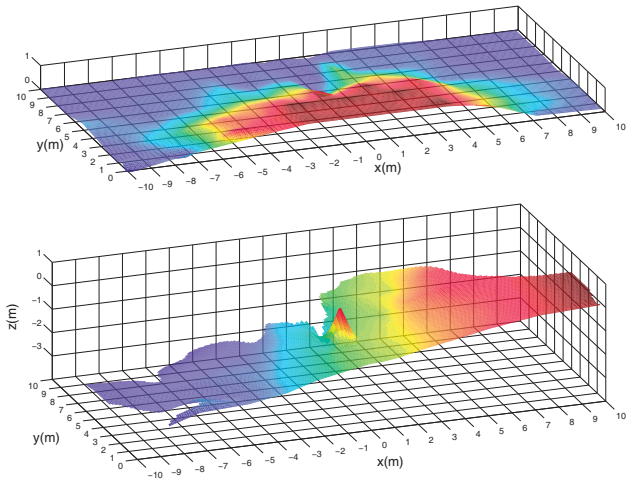

Fig. 7. Top: fuzzy reliability mask of the close-front obstacle scene with $p = 0.5$. Bottom: Application of the mask to the elevation map with 15×8 rules for $v \geq 0.1$.

computed for the close-front obstacle scene with $p = 0.5$ and $\delta = 0.1\,\mathrm{m}$ as well as its to the ANFIS model of 15×8 rules with $v \geq 0.1$. The result is a reliable fuzzy elevation map without modelling artifacts.

4 Conclusions

This paper has addressed terrain modeling with fuzzy elevation maps from a ground-based 3D laser scan. Fuzzy surfaces provide a non-discrete representation of terrain elevation that greatly reduces the number of parameters with respect to raw point clouds. In particular, substantial performance improvements over [23] have been contributed. Proposed enhancements are spherical sub-sampling for training data selection, triangular membership functions with standard fuzzy partition, and zero order Sugeno-type inference. Furthermore, the problem of fuzzy surface artifacts in shadowed regions has been addressed by computing a fuzzy reliability mask from the same set of sub-sampled data.

Scans from a Hokuyo-based 3D rangefinder have been used to model natural terrain with and without salient obstacles. The proposed method outperforms QSlim and the previous ANFIS model in the adjustment to the original scan data, as indicated by the root mean squared error, especially with close obstacles. Besides, the new solution reduces significantly the number of model parameters. Future work will explore fuzzy identification with no predefined structure.

Acknowledgements

This work was partially supported by the Spanish CICYT project DPI 2011-22443 and the Andalusian project PE-2010 TEP-6101.

References

1. J. Serón, J. L. Martínez, A. Mandow, A. J. Reina, J. Morales, and A. García-Cerezo, "Automation of the arm-aided climbing maneuver for tracked mobile manipulators," *IEEE Transactions on Industrial Electronics*, vol. 61, no. 7, pp. 3638–3647, 2014.
2. A. Santamaria-Navarro, E. H. Teniente, M. Morta, and J. Andrade-Cetto, "Terrain classification in complex three-dimensional outdoor environments," *Journal of Field Robotics*, vol. 32, no. 1, pp. 42–60, 2015.
3. C. H. Tong, T. D. Barfoot, and E. Dupuis, "Three-dimensional SLAM for mapping planetary work site environments," *Journal of Field Robotics*, vol. 29, no. 3, pp. 381–412, 2012.
4. I. Rekleitis, J.-L. Bedwani, E. Dupuis, T. Lamarche, and P. Allard, "Autonomous over-the-horizon navigation using LIDAR data," *Autonomous Robots*, pp. 1–18, 2012.
5. G. Ishigami, M. Otsuki, and T. Kubota, "Path planning and navigation framework for a planetary exploration rover using a laser range finder," *Springer Tracts in Advanced Robotics*, vol. 92, pp. 431–447, 2014.
6. K. Nagatani, N. Tokunaga, Y. Okada, K. Yoshida, Y. Hada, T. Yoshida, and E. Koyanagi, "Teleoperation of all-terrain robot using continuous acquisition of three-dimensional environment under time-delayed narrow bandwidth communication," in *IEEE Int. Workshop on Safety, Security & Rescue Robotics*, Denver, USA, 2009.
7. A. Birk, K. Pathak, N. Vaskevicius, M. Pfingsthorn, J. Poppinga, and S. Schwertfeger, "Surface representations for 3D mapping," *Künstliche Intelligenz*, vol. 24, pp. 249–254, 2010.
8. D. Gingras, T. Lamarche, J. L. Bedwani, and E. Dupuis, "Rough terrain reconstruction for rover motion planning," in *Proc. Canadian Conference on Computer and Robot Vision*, Ottawa, Canada, 2010, pp. 191 – 198.
9. N. Vaskevicius, A. Birk, K. Pathak, and S. Schwertfeger, "Efficient representation in three-dimensional environment modeling for planetary robotic exploration," *Advanced Robotics*, vol. 24, no. 8-9, pp. 1169–1197, 2010.
10. P. Pfaff, R. Triebel, and W. Burgard, "An efficient extension to elevation maps for outdoor terrain mapping and loop closing," *Int. Journal of Robotics Research*, vol. 26, no. 2, pp. 217–230, 2007.
11. G. Ishigami, K. Nagatani, and K. Yoshida, "Path planning and evaluation for planetary rovers based on dynamic mobility index," in *IEEE Int. Conf. on Intelligent Robots and Systems*, 2011, pp. 601–606.
12. A. Souza and L. M. G. Gonalves, "Occupancy-elevation grid: an alternative approach for robotic mapping and navigation," *Robotica*, 2015.
13. T. Gerbaud, V. Polotski, and P. Cohen, "Simultaneous exploration and 3D mapping of unstructured environments," in *IEEE Int. Conf. on Systems, Man and Cybernetics*, vol. 6, 2004, pp. 5333–5337.
14. A. Ciampalini, P. Cignoni, C. Montani, and R. Scopigno, "Multiresolution decimation based on global error," *The Visual Computer*, vol. 13, pp. 228–246, 1997.
15. M. Garland and P. S. Heckbert, "Surface simplification using quadric error metrics," in *ACM SIGGRAPH Conf. on Computer Graphics*, 1997, pp. 209–216.
16. J. Santos, W. A. Lodwick, and A. Neumaier, "A new approach to incorporate uncertainty in terrain modeling," in *2nd Int. Conf. on Geographic Information Science*, Boulder, USA, 2002, pp. 291–299.

17. M. Anile, P. Furno, G. Gallo, and A. Massolo, "A fuzzy approach to visibility maps creation over digital terrains," *Fuzzy Sets and Systems*, vol. 135, pp. 63 –80, 2003.
18. H. Liu, J. Yang, and C. Zhao, "A generic approach to rugged terrain analysis based on fuzzy inference," in *8th Int. Conf. on Control, Automation, Robotics and Vision*, vol. 2, 2004, pp. 1108–1113.
19. J. Gu, Q. Cao, and Y. Huang, "Rapid traversability assessment in 2.5D grid-based map on rough terrain," *Int. Journal of Advanced Robotic Systems*, vol. 5, no. 4, pp. 389–394, 2008.
20. S. Vasudevan, F. Ramos, E. Nettleton, and H. Durrant-Whyte, "Gaussian process modeling of large scale terrain," *Journal of Field Robotics*, vol. 26, no. 10, pp. 812 – 840, 2009.
21. J.-S. R. Jang, "ANFIS: Adaptative-network-based fuzzy inference system," *IEEE Transactions on Systems, Man and Cybernetics*, vol. 23, no. 3, pp. 665–685, 1993.
22. F. Samadzadegan, A. Azizi, M. Hahn, and C. Lucas, "Automatic 3D object recognition and reconstruction based on neuro-fuzzy modelling," *ISPRS Journal of Photogrammetry and Remote Sensing*, vol. 59, no. 5, pp. 255–277, 2005.
23. A. Mandow, T. J. Cantador, A. García-Cerezo, A. J. Reina, J. L. Martínez, and J. Morales, "Fuzzy modeling of natural terrain elevation from a 3D scanner point cloud," in *7th IEEE Int. Symposium on Intelligent Signal Processing (WISP)*, Floriana, Malta, 2011.
24. J.-L. Martínez, A. Mandow, A. Reina, T.-J. Cantador, J. Morales, and A. García-Cerezo, "Navigability analysis of natural terrains with fuzzy elevation maps from ground-based 3D range scans," in *Proc. IEEE/RSJ International Conference on Intelligent Robots and Systems*, Tokyo, Japan, 2013, pp. 1576–1581.
25. A. Mandow, J. L. Martnez, A. J. Reina, and J. Morales, "Fast range-independent spherical subsampling of 3D laser scanner points and data reduction performance evaluation for scene registration," *Pattern Recognition Letters*, vol. 31, no. 11, pp. 1239 – 1250, 2010.
26. Z.-H. Xiu and G. Ren, "Stability analysis and systematic design of Takagi-Sugeno fuzzy control systems," *Fuzzy Sets and Systems*, vol. 151, no. 1, pp. 119 – 138, 2005.
27. J. Morales, J. L. Martínez, A. Mandow, A. J. Reina, A. Pequeño Boter, and A. García-Cerezo, "Boresight calibration of construction misalignments for 3D scanners built with a 2D laser rangefinder rotating on its optical center," *Sensors*, vol. 14, no. 11, pp. 20 025–20 040, 2014.
28. N. Derbel, "A discussion on Sugeno fuzzy logic approximations of nonlinear systems," in *5th Int. Multi-Conf. on Systems, Signals and Devices*, Amman, Jordan, 2008.
29. J.-S. R. Jang, C.-T. Sun, and E. Mizutani, *Neuro-fuzzy and soft computing: a computational approach to learning and machine intelligence.* Prentice Hall, 1997.
30. J. Morales, J. L. Martínez, A. Mandow, A. Pequeo-Boter, and A. García-Cerezo, "Design and development of a fast and precise low-cost 3D laser rangefinder," in *IEEE Int. Conf. on Mechatronics*, Istanbul, Turkey, 2011, pp. 621 – 626.
31. C. Little and R. Peters, "Simulated mobile self-location using 3D range sensing and an a-priori map," in *Proc. IEEE International Conference on Robotics and Automation*, vol. 2005, Barcelona, Spain, 2005, pp. 1459–1464.
32. A. Biniaz, "Slope preserving terrain simplification - an experimental study," in *Proc. Canadian Conference on Computational Geometry*, Vancouver, Canada, 2009, pp. 59–62.